Active impedance control optimization for attenuation of acoustic cavity modes

Emanuele de Bono, Davide Ponticelli, Sergio de Rosa, Giuseppe Petrone, Morvan Ouisse, Rafael Teloli

Active impedance control optimization for attenuation of acoustic cavity modes

E. De Bono*[1], D. Ponticelli†[2], S. De Rosa‡[2], G. Petrone§[2], M. Ouisse¶[3], and R. Teloli‖[3]

[1]Univ Lyon, CNRS, École Centrale de Lyon, LTDS, UMR5513, 69130 Ecully, France.
[2]Laboratory for Promoting Experiences in Aeronautical Structures and Acoustics, Department of Industrial Engineering, Università degli Studi di Napoli "Federico II," Via Claudio 21, Napoli, 80125, Italy.
[3]SUPMICROTECH, Université de Franche-Comté, CNRS, institut FEMTO-ST, F-25000 Besançon, France.

August 17, 2024

Abstract

Cavity noise control is a highly demanded research field for the manipulation of noise in vehicle interiors. A very ambitious application is the aircraft fuselage, presenting many challenges related to the simultaneous necessity of blocking sound transmission and absorbing acoustic energy, while fulfilling strict weight and spatial constraints. Many innovative solutions are being investigated, such as subwavelength resonators, porous materials and hybrid composites combining resonant and porous elements. Also, classical active noise cancellation has a vast literature for controlling cavity noises in vehicle interiors. The active impedance control concept instead, with its advantages related to inherent acoustical passivity and stability, has recently prompted its technological readiness level, but still lacks of proper optimization models. Generally, in acoustics, a surface is used to be characterized in terms of its impedance and absorption coefficient. The consequent optimization is based upon the maximization of the absorption

*Post-doctoral researcher, LTDS École Centrale de Lyon, emanueledeb88hotmail.it.
†Engineer, Geven, davide.ponticelli@live.it.
‡Professor, DII, University Federico II of Naples, derosa@unina.it.
§Assistant Professor, DII, University Federico II of Naples, giuseppe.petrone@unina.it.
¶Professor, DMA, Université de Franche-Comté, morvan.ouisse@femto-st.fr.
‖Associate Professor, DMA, Université de Franche-Comté, rafael.teloli@femto-st.fr.

coefficient, which means the minimization of the reflected sound field. Nevertheless, the criteria for optimal damping of acoustic cavities, either at a single frequency or in a frequency bandwidth, do not coincide with the maximization of absorption coefficient in the corresponding frequencies of interest. This is due to the impact of the surface impedance scattering upon the global sound pressure field in the acoustic cavity. In the sound scattering, an equal role is played by both resistive and reactive impedance components. For this reason, the optimal resistance depends upon the reactance, as it is the case for the equivalent well known problem in solid mechanics, of Tuned Mass Damper optimization. In this paper, we discuss the significance of absorption maximization in comparison with classical modal damping optimization criteria coming from the solid mechanics literature. Finally, a preliminary test-bench has been built in order to test the impedance control in a small acoustic environment treated on one side by electroacoustic resonators, and preliminary modal attenuation results are discussed.

1 Introduction

The control of noise in acoustic cavities is a research field which interests various industrial domains: from building acoustics, to automotive and aeronautics. Among them, fuselage noise insulation presents the hardest challenges, notoriously because of weight and spatial strict constraints. A double task is demanded for fuselage noise control: to block sound transmission from external sources, and to absorb noise from internal source paths [1]. Large efforts have been carried out to conceive innovative materials able to achieve higher sound insulation performances within limited thickness [2, 3], usually exploiting the potentialities of porous materials [4], resonators [5], or a combination of them [6, 7]. Parallelly, the suppression of structural vibration is under study and several solutions have been proposed, such as periodic inclusions [8]. Active vibration suppression is another interesting avenue, as proposed in [9–11] for both automotive and aeronautic applications. In [12], the potentialities of active noise control is examined both in terms of structural actuators and secondary noise sources. The active noise cancellation is recently being investigated toward the integration of machine learning algorithms in adaptive architectures [13]. In the technological prospective of miniaturization, artificial intelligence integration and weight reduction, along with the well-established digitalization and fast-computing performances, active noise control is progressively gaining interest. In particular, the active impedance control architecture and the so-called Electroacoustic Resonators (ERs) allows to assure passivity and stability [14], and has been recently been employed to target also nonlinear [15–20] and nonlocal behaviours [21–28], stepping forward in the Technological Readiness Level (TRL). In particular, nonlocal boundary operators offer unprecedented research avenues compared to classical local impedance control strategies, to envisage unconventional designs for noise control in acoustic cavities. The preliminary design and optimization of nonlocal absorbers would very much benefit from a wave propagation description

of the acoustic field. In acoustics, the absorption coefficient is the most employed parameter employed to characterize the efficiency of a surface impedance, and the optimal value for total absorption is a well-known result [29], for any angle of incidence of plane waves, except for the grazing incidence case. Nevertheless, maximum absorption of plane waves in a limited frequency range, does not assure maximum attenuation of the frequency response of the main system (the acoustic cavity) in the frequency band of interest. This is due to the impact of the surface impedance scattering upon the global sound pressure field in the acoustic cavity. In the sound scattering, an equal role is played by both resistive and reactive impedance components. For this reason, the optimal resistance depends upon the reactance, as it is the case for the equivalent well known problem in solid mechanics, of Tuned Mass Damper (TMD) optimization. From single-degree-of-freedom (SDOF) main structures [30, 31], to multimodal domain extensions [32–34], Den Hartog equal peak gave the bases for maximizing the attenuation of the main system modes. Other optimization methods have then been designed for spatially distributed TMDs [35], and noise radiation in enclosed acoustic cavities [36], based upon minimization of global metrics describing the response of the main system.
However, in acoustics, sufficient literature upon the optimization of cavity noise control is not equally satisfactory, to the authors knowledge. In the present paper, we first discuss the relevance of single modal damping optimization analyses based only on the resistive component of the surface impedance [37]. The habit of considering purely resistive impedances comes from the maximization of the absorption coefficient of acoustic resonators, where the maximum value is only given by the resistive component of the surface impedance. The Plane-Wave-Decomposition (PWD) applied to any cavity shape [38] (showed in Section 2) allows the correlation of the optimal resistive impedance to the maximization of modal damping, as showed by the numerical simulations of Section 3. Nevertheless, the presence of a reactive component requires a complexification of this approach, to take into account the contribution of the scattered fields, which is out of the scope of the present contribution. In Section 4, we analyse a 1D cavity problem to highlight the limits of the absorption coefficient approach on an analytical case study. Finally, in Section 5, we report some preliminary experimental results in two test-benches: a monomodal and a multi-modal cavity, to confirm the previous inferences and demonstrate the tunability of our local impedance control. The main interest of this contribution relies in providing the necessary analytical, numerical and experimental background to envisage advanced optimization strategies for cavity noise control, such as those based upon the Reinforcement Learning.

2 The Plane-Wave-Decomposition

The sound field into an acoustic cavity, can be decomposed upon its modal basis, as in Eq. (1):

$$p(\vec{x},t) = \sum_{n=1}^{N} A_n \psi_n(\vec{x})\, e^{\mathrm{j}\Omega_n t}, \tag{1}$$

where $\psi_n(\vec{x})$ are the modal shape function, $\vec{x} = x\hat{x} + y\hat{y} + z\hat{z}$ is the position vector, A_n are the participation factors of each mode, and Ω_n the corresponding complex eigenfrequencies multiplying the time variable t. We can decompose $\Omega_n = \omega_n + \mathrm{j}\delta_n$ in its real (natural angular frequency ω_n) and imaginary part (modal damping coefficient δ_n). From the approximation of Helmholtz solutions by generalized harmonic polynomials [39], it is possible to further decompose each mode shape function into its plane wave components, as in Eq. (2).

$$\psi_n(\vec{x},t) = \sum_{r=1}^{R} B_{nr}\, e^{-\mathrm{j}\vec{k}_{nr}\cdot\vec{x}}. \tag{2}$$

In Eq. (2), $\vec{k}_{nr}$ are the wavevectors with amplitude $|k_n| = |\Omega_n|/c_0$ (c_0 is the speed of sound) and direction $\vec{r}$ in space, while B_{nr} are the expansion coefficients of $\psi_n(\vec{x})$ along the directions $\vec{r}$. Replacing Eq. (2) into Eq. (1), we obtain:

$$p(\vec{x},t) = \sum_{n=1}^{N} A_n e^{\mathrm{j}\Omega_n t} \sum_{r} B_{nr}\, e^{-\mathrm{j}\vec{k}_{nr}\cdot\vec{x}} = \sum_{n=1}^{N}\sum_{r=1}^{R} C_{nr} e^{\mathrm{j}\Omega_n t - \mathrm{j}\vec{k}_{nr}\cdot\vec{x}}, \tag{3}$$

with $C_{nr} = A_n B_{nr}$ the participation factors to the system response $p(\vec{x},t)$, of each plane wave described by $\vec{k}_{nr}$. Each exponential function of Eq. (3) describes the wave propagation along $\vec{k}_{nr}$. They constitute the functional basis of the PWD, which, unlike the modal decomposition, has an explicit form [38]. As the of modes N employed in Eq. (1) determines the level of accuracy of the modal decomposition, analogously, the number R of plane wave directions employed in Eq. (2) determines the accuracy of the PWD. A good choice for the directions r is an uniform sampling [38] on the sphere of radius $|k_n|$.

3 2D simulations

Let us start with the simplest case of a 2D rectangular acoustic cavity of sizes L_x, L_y with rigid walls. In that case, the mode shapes have the analytical form:

$$\psi_{m,n}(x,y) = \cos\left(\frac{m\pi x}{L_x}\right)\cos\left(\frac{n\pi y}{L_y}\right), \tag{4}$$

where the indices m, n assume the values $m = 0, 1, 2, 3...$ and $n = 0, 1, 2, 3...$. Eq. (4) can be rewritten in terms of plane waves, as:

$$\psi_{m,n}(x,y) = A_1 e^{\mathrm{j}k_{x,1}x} + A_2 e^{\mathrm{j}k_{x,2}x} + B_1 e^{\mathrm{j}k_{y,1}y} + B_2 e^{\mathrm{j}k_{y,2}y}, \tag{5}$$

with $k_{x,1} = -k_{x,2} = m\pi/L_x$, $k_{y,1} = -k_{y,2} = n\pi/L_y$, and $A_1 = -A_2$, $B_1 = -B_2$. Eq. (5) is the PWD of the acoustic modes of a rectangular

cavity. From Eq. (5), we can easily retrieve the main directions of plane wave propagation, also called elevation angles $\theta_{m,n}$ [40]:

$$\theta^{(1)}_{m,n} = atan\left(\frac{k_{y,1}}{k_{x,1}}\right) = atan\left(\frac{nL_x}{mL_y}\right); \tag{6a}$$

$$\theta^{(2)}_{m,n} = atan\left(\frac{k_{y,2}}{k_{x,2}}\right) = -\theta^{(1)}_{m,n}; \tag{6b}$$

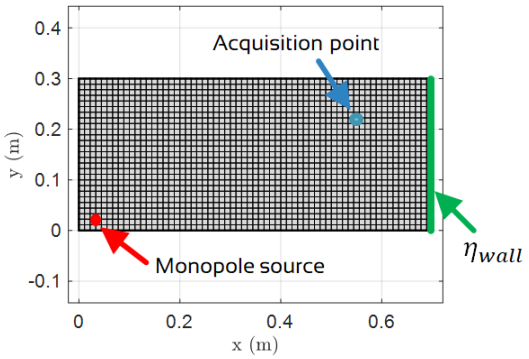

Figure 1. Finite Element mesh of the 2D rectangular cavity with positions of the monopole source and the acquisition point, treated on one side by the normalized mobility η_{wall}.

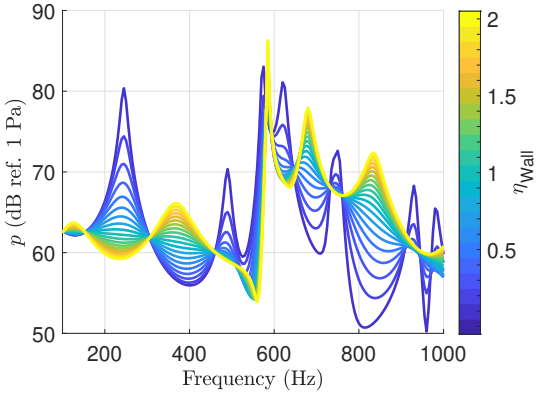

Figure 2. Frequency response at the measurement point, for a monopole source of volume flow rate per unit length $Q = 1$ m^2/s, and varying η_{wall}.

In open field, we know [41] that plane waves impacting a surface with incident angle $\theta^{(1)}_{m,n}$ are totally absorbed if the surface exhibits a local surface impedance $Z^{opt}_{wall} = \rho_0 c_0 / \cos\theta^{(1)}_{m,n}$, where ρ_0 is the static air density. Observe that $\cos\theta^{(1)}_{m,n} = \cos\theta^{(2)}_{m,n}$, therefore we can drop the superscript and refer directly to $\cos\theta_{m,n}$. In

terms of normalized mobility $\eta_{wall} = \rho_0 c_0 / Z_{wall}$, we have $\eta_{wall}^{opt} = \cos\theta_{m,n}$. As long as the PWD holds, we expect maximum attenuation of mode m, n if an entire wall of the cavity is treated by η_{wall}^{opt}. In order to check the validity of such inference, we can analyse the frequency response of our rectangular cavity, subjected to a monopole source, and with a wall treated by varying η_{wall}, as showed in Fig. 1.

Fig. 2 shows the frequency response obtained by Finite Elements (FEs) in Comsol, for a monopole source with volume flow rate per unit length $Q = 1$ m^2/s, and varying η_{wall} from 0.1 to 2. Notice that for very law values of η_{wall} we approach the condition of rigid wall, which presents resonance frequencies given by $f_{res}^{Rigid} = \frac{c_0}{2}\sqrt{\frac{m^2}{L_x^2} + \frac{n^2}{L_y^2}}$, with $m = 1, 2, 3...$ and $n = 1, 2, 3....$ Instead, by increasing η_{wall} we approach the open condition, and the resonance frequencies for a rectangular cavity with one open end (and all the other rigid) are $f_{res}^{Open} = \frac{c_0}{2}\sqrt{\frac{m^2}{4L_x^2} + \frac{n^2}{L_y^2}}$, with $m = 0, 1, 3, 5...$ and $n = 0, 1, 2, 3...$. This explains why some resonances are exchanged with antiresonances when η_{wall} moves from the lowest to the highest values.

Let us now focus on the frequency range dominated by longitudinal modes, i.e. $n = 0$ and $\theta_{m,0} = 0$. According to the above inference, $\eta_{wall}^{opt} = \cos\theta_{m,n} = 1$. On top of Fig. 3 the frequency response in the frequency range dominated by longitudinal modes is showed for few values of η_{wall}. Observe how for $\eta_{wall} = 1$ (in solid green), the resonances and antiresonances disappears, as total absorption is achieved at the treated boundary. On bottom of Fig. 3, we identify the values of $\cos\theta_{m,n}$ at the resonance frequencies, in case of untreated (rigid) wall.

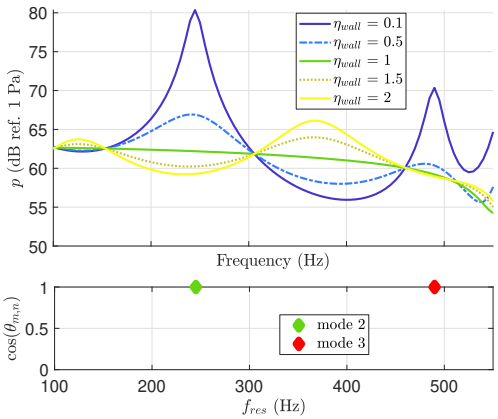

Figure 3. Frequency response at the measurement point, with varying η_{wall} (top), and $\cos\theta_{m,n}$ at the resonance frequencies f_{res} in the rigid case (bottom), between 100 and 550 Hz.

Fig. 4 focuses on the frequency range between 600 and 900 Hz, where modes with $n \neq 0$ (of the rigid case) are dominant. At the bottom of Fig. 4, the $\cos\theta_{m,n}$ is plotted against the corresponding resonance frequencies f_{res}, in case of untreated (rigid) wall. The acoustic cavity with fully rigid walls

present three modes in this frequency range, corresponding to values of $\cos\theta_{m,n}$ equal to 0.4, 0.65 and 1, for modes 5, 6 and 7, respectively. On top of Fig. 4, the frequency response is plotted for several values of η_{wall}. Observe how, for $\eta_{wall} = 1$, the resonances are not annihilated. The values of η_{wall} equal to 0.4 and 0.6, corresponding to approximately the total absorption condition for $\theta_{m,n}$ of modes 5 and 7, present significant attenuation. In particular, $\eta_{wall} = 0.4$ totally eliminates the resonance of mode 5, while being suboptimal around 730 Hz, where a longitudinal mode is dominant ($\cos\theta_{m,n} = 0$ for mode 6). The presence of multiple principal direction of propagation in a narrow bandwidth, entails delicate optimization processes, which can nevertheless benefit from the PWD. This analysis provide an interesting perspective to physically interpret the results reported in [37].

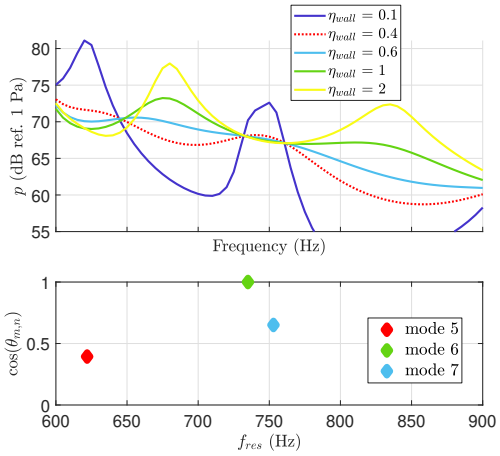

Figure 4. Frequency response at the measurement point, with varying η_{wall} (top), and $\cos\theta_{m,n}$ at the resonance frequencies f_{res} in the rigid case (bottom), between 600 and 900 Hz.

Nevertheless, purely real impedances are not physically realisable as they do not respect the *reality* condition [42]. As complex impedances, such as resonators, are of concern, a significant complexification of this approach is required, where the impact of the surface impedance on both incident and scattered plane waves of the frequency response must be taken into account. This is out of the scope of the present paper. In the next section, we demonstrate the limitations of the approach based upon the maximization of the absorption coefficient, in a simple 1D case study.

4 Maximum absorption versus optimal modal damping

Let us consider an acoustic cavity, where only 1D propagation is allowed, as the one in Figure 5.

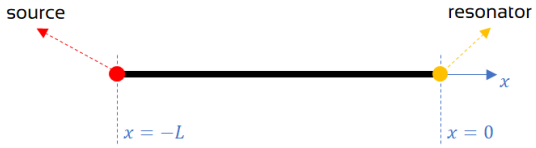

Figure 5. Sketch of the 1D cavity.

The boundary conditions are: $\tilde{v}(x=-L)=v_0$ and $\tilde{v}(x=0)=\tilde{p}(x=0)/Z_{ER}$, where v is the acoustical velocity along x and Z_{ER} the acoustic impedance of a SDOF resonator. This problem can be solved analytically in frequency domain, giving:

$$\tilde{p}(x,\omega)=\rho_0 c_0 v_0 \frac{e^{-\mathrm{j}k_0 x}+Re^{\mathrm{j}k_0 x}}{e^{\mathrm{j}k_0 L}-Re^{-\mathrm{j}k_0 L}}, \tag{7}$$

where $R=(Z_{ER}-\rho_0 c_0)/(Z_{ER}+\rho_0 c_0)$. The resonator SDOF impedance reads:

$$Z_{ER}(\mathrm{j}\omega)=M_{ER}\mathrm{j}\omega+R_{ER}+\frac{K_{ER}}{\mathrm{j}\omega}, \tag{8}$$

where M_{ER}, R_{ER} and K_{ER} are the mass, resistance and stiffness coefficients. In order to keep the same values as the experimental ERs, we define $M_{ER}=\mu_M M_0$ and $K_{ER}=\mu_K K_0$, where M_0 and K_0 are the mass and stiffness of the electroacoustic resonator without control. Their values are $M_0=0.354$ kg/m^2 and $K_0=3.067\times10^6$ Pa/m.

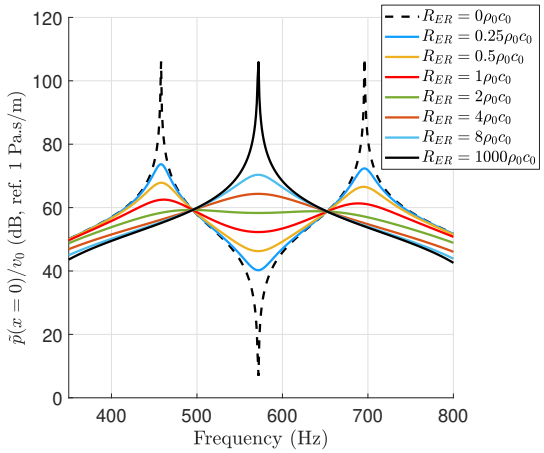

Figure 6. Frequency response of the sound pressure field at $x=0$ divided by v_0, around the first resonance.

In Figure 6, we show the analytical frequency response of the sound pressure at $x=0$ divided v_0, in case of $\mu_M=1$ and μ_K such that the resonant frequency

of the resonator coincides with the first resonance of the 1D cavity. Apparently, the optimal damping for the attenuation of the first mode is close to $2\rho_0 c_0$. From this simple calculation we can verify that the maximum absorption condition at resonance, given by $R_{ER} = \rho_0 c_0$, does not correspond to the optimal damping of the mode, as the two side-peaks are enhanced.

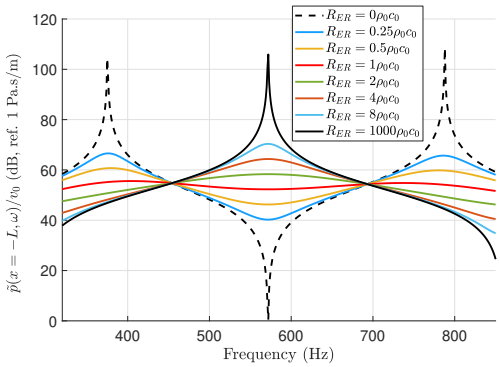

Figure 7. Frequency response of the sound pressure field at $x = 0$ divided by v_0, around the first resonance.

Figure 7 shows the same frequency response in case of $\mu_M = 0.2$. As expected, the efficient bandwidth is enlarged, while the optimal resistance is reduced to a value close to $R_{ER} = \rho_0 c_0$. Indeed, by reducing the mass term (and therefore the stiffness term as well), the reactive component becomes less important and we approach the condition of purely resistive impedance for which the maximum absorption criteria coincides with the maximum modal damping. In the next section, we discuss some preliminary result of tunable ERs lining a wall of a small cavity.

5 Experimental results

In order to experimentally test cavity modes attenuation by impedance control, we have employed the ERs. Each ER is composed of a speaker (the actuator) and four microphones able to retrieve the average pressure on the speaker diaphragm. Each sides of the cell measures about 5 cm, with a speaker diameter of about 4 cm. By a programmable digital control algorithm, it is possible to enforce the electrical current in the ER speaker coil based upon the measured pressure, so that to drive the velocity of the speaker membrane and achieve a desired surface impedance on the diaphragm. The control algorithm is based upon the model-inversion strategy, and is detailed in [14] along with some elements of its electronic architecture. The surface acoustic impedance targeted by the control algorithm has the form:

$$Z_d(\mathrm{j}\omega) = M_d \mathrm{j}\omega + r_d \rho_0 c_0 + \frac{K_d}{\mathrm{j}\omega}, \tag{9}$$

where M_d is the desired acoustic mass, r_d is the desired acoustic resistance normalized to $\rho_0 c_0$, and K_d is the desired acoustic stiffness.

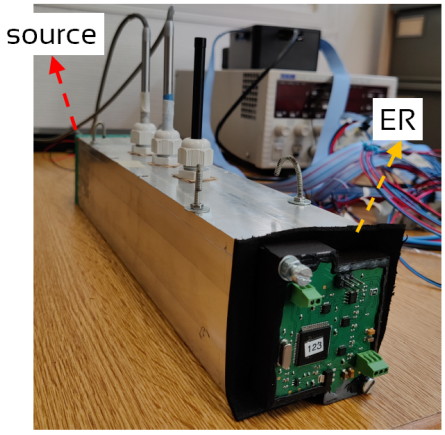

Figure 8. Photo of the 1D acoustic cavity.

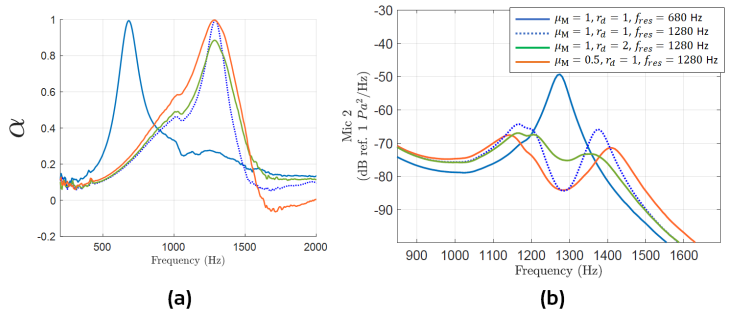

Figure 9. Absorption coefficient spectra **(a)** and Power-Spectral-Density **(b)** of sound pressure at one microphone in the frequency range around 1250 Hz, for various target resistances.

The first test-bench is the classical Kundt's tube, see Figure 8, where only 1D propagation is involved in the frequency range of interest. The conclusions of the previous section are confirmed by the results showed in Figure 9. The case of a resonance frequency $f_{res} = 680$ Hz is compared to the case of targeting 1280 Hz, to demonstrate the tunability of our ER. Around 1280 Hz, a mode of the 1D cavity is present, which explains the peak of the Power-Spectral-Density (PSD) when the ER resonance is placed at 680 Hz, and its impact on the cavity response is very low. By targeting 1280 Hz, the corresponding resonance is attenuated. As expected, the case of $r_d = 1$ entails more significant side-peaks

with respect to the case of $r_d = 2$. Instead, by reducing the mass term μ_M from 1 to 0.5, it is possible to enlarge the bandwidth, attenuate the original peak along with the side-peaks, for $r_d = 1$. This confirms the above discussion about the dependence of the optimal resistance upon the mass coefficient.

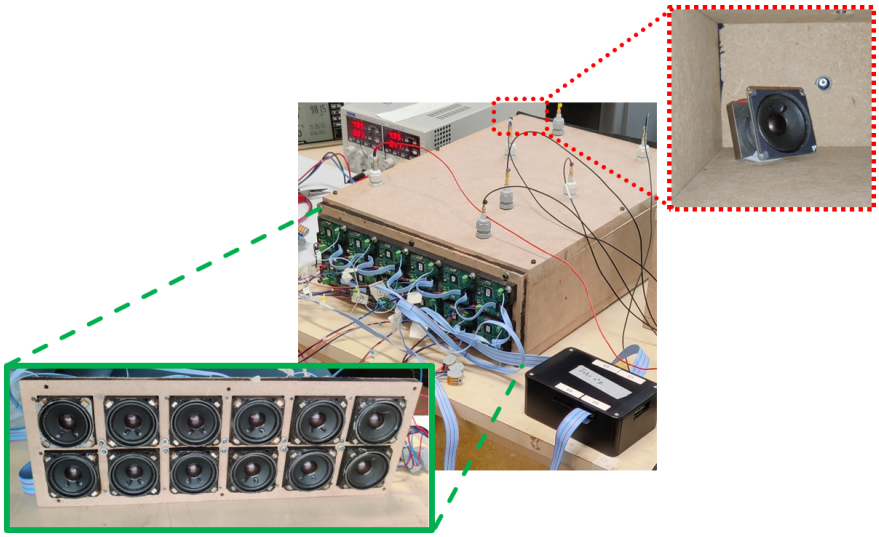

Figure 10. Experimental test-bench: box cavity with randomly placed acquisition points, lined wall (bottom-left) and noise source (top right).

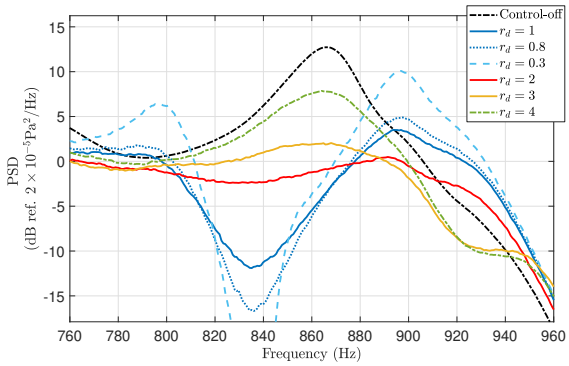

Figure 11. Power-Spectral-Density of sound pressure at one microphone location in the frequency range 760-960 Hz (top), for various target resistances.

The second experimental setup to test the cavity modes control is a small box made up of wood, of dimensions $L_x = 0.5$ m, $L_y = 0.35$ m, $L_z = 0.105$ m, with randomly placed microphones, as it is showed in Fig. 10. One face of the cavity is treated by 12 ERs covering almost the entire surface of size $L_y \times L_z$. A noise source is placed on a corner of the opposite face. Fig. 11 shows the PSD of the sound pressure at one microphone location, in the frequency range

760-960 Hz, for various target normalized resistances r_d. The target acoustic mass is fixed, while the desired acoustic stiffness is adjusted to tune the resonance frequency of $Z_d(\mathrm{j}\omega)$ to about 840 Hz, which is the natural frequency of mode 6 dominating this bandwidth, in case of rigid walls. The PSDs are compared to the case of no-control applied to the ERs (Control-off), which leads the ERs to feature a mass-like behaviour at these frequencies. From Fig. 10, the maximum attenuation at resonance, with minimum impact on the side peaks, looks to be achieved for values close to $r_d = 2$.

6 Conclusions

In this paper, we have discussed the significance of the absorption coefficient parameter to assess the optimal behaviour of a resonator in an acoustic cavity. The optimal absorption for oblique plane waves can be correlated to the maximum cavity mode attenuation, in case of purely resistive impedances, thanks to the Plane Wave Decomposition, as described in Section 2. Nevertheless, the research of an optimal purely resistive impedance, as done in [37], is not significant when resonators are concerned (and in general when the reactive terms cannot be discarded). This is demonstrated on a simple 1D case study in Section 4: only when the mass term (and therefore the reactive component) of the impedance becomes very low, the optimal resistance can be approximated by the one providing the unit absorption at the resonator resonance. Then, a 1D experimental test-bench with an Electroaoustic Resonator is employed for parametrically varying the resistance of the resonator, confirming the previous conclusions. Finally, a multi-modal acoustic cavity is employed to test the tunability of our Electroacoustic Resonators. Next steps will involve the derivation of the optimal mass-dependent resistance by applying the equal peak method as in solid mechanics [30], and the study of the effect of the acoustically treated surface on both monomodal and multimodal environments. These tools will provide comparison case-studies for the testing of reinforcement-learning optimization algorithms.

References

[1] Harvey H Hubbard. *Aeroacoustics of flight vehicles: theory and practice*, volume 1. National Aeronautics and Space Administration, Office of Management∼. . . , 1991.

[2] Min Yang and Ping Sheng. Sound absorption structures: From porous media to acoustic metamaterials. *Annual Review of Materials Research*, 47:83–114, 2017.

[3] Giorgio Palma, Huina Mao, Lorenzo Burghignoli, Peter Göransson, and Umberto Iemma. Acoustic metamaterials in aeronautics. *Applied Sciences (Switzerland)*, 8(6):971, 2018.

[4] Zacharie Laly, Noureddine Atalla, Raymond Panneton, Sebastian Ghinet, and Christopher Mechefske. Finite Element Study of Perfect Sound Absorbing Porous Material with Periodic Conical Hole Profile. *Canadian Acoustics*, 51(3):134–135, 2023.

[5] Giuseppe Catapane, Giuseppe Petrone, and Olivier Robin. Series and parallel coupling of 3D printed micro-perforated panels and coiled quarter wavelength tubes. *The Journal of the Acoustical Society of America*, 154(5):3027–3040, 2023.

[6] Tenon Charly Kone, Sebastian Ghinet, Raymond Panneton, and Anant Grewal. Broadband low frequency noise attenuation using thin acoustic metamaterials for aircraft cabin noise mitigation. In *INTER-NOISE and NOISE-CON Congress and Conference Proceedings*, volume 268, pages 3223–3231. Institute of Noise Control Engineering, 2023.

[7] Claude Boutin and François Xavier Becot. Theory and experiments on poro-acoustics with inner resonators. *Wave Motion*, 54:76–99, 2015.

[8] Christophe Droz, Olivier Robin, Mohamed Ichchou, and Noureddine Atalla. Improving sound transmission loss at ring frequency of a curved panel using tunable 3D-printed small-scale resonators. *The Journal of the Acoustical Society of America*, 145(1):EL72—-EL78, 2019.

[9] Malte Misol, Stephan Algermissen, Hans Peter Monner, and Anja Naake. Reduction of interior noise in an automobile passenger compartment by means of active structural acoustic control (ASAC). *Proceedings of NAG/DAGA 2009*, 2009.

[10] Malte Misol, Thomas Haase, Hans Peter Monner, and Michael Sinapius. Causal feedforward control of a stochastically excited fuselage structure with active sidewall panel. *The Journal of the Acoustical Society of America*, 136(4):1610–1618, 2014.

[11] Malte Misol and Stephan Algermissen. Noise reduction results of the ACASIAS Active Lining Panel. 2020.

[12] Paolo Gardonio and Stephen John Elliott. Active control of structure-borne and airborne sound transmission through double panel. *Journal of Aircraft*, 36(6):1023–1032, 1999.

[13] Young-Jin Cha, Alireza Mostafavi, and Sukhpreet S Benipal. DNoiseNet: Deep learning-based feedback active noise control in various noisy environments. *Engineering Applications of Artificial Intelligence*, 121:105971, 2023.

[14] E. De Bono, M. Collet, G. Matten, S. Karkar, H. Lissek, M. Ouisse, K. Billon, T. Laurence, and M. Volery. Effect of time delay on the impedance control of a pressure-based, current-driven Electroacoustic Absorber. *Journal of Sound and Vibration*, 537:117201, 2022.

[15] E. De Bono, M. Morell, M. Collet, E. Gourdon, A. Ture Savadkoohi, M. Ouisse, and C. H. Lamarque. Model-inversion control to enforce tunable Duffing-like acoustical response on an Electroacoustic resonator at low excitation levels. *Journal of Sound and Vibration*, 570:118070, feb 2024.

[16] Maxime Morell, Emmanuel Gourdon, Manuel Collet, Alireza Ture Savadkoohi, Emanuele De Bono, and Claude-Henri Lamarque. Towards digitally programmed nonlinear electroacoustic resonators for low amplitude sound pressure levels: Modeling and experiments. *Journal of Sound and Vibration*, 584:118437, 2024.

[17] Camila Elizabeth da Silveira Zanin, Aurélie Labetoulle, Emanuele De Bono, Emmanuel Gourdon, Manuel Collet, and Alireza Ture Savadkoohi. Experimental evidences of nonlinear programmable electroacoustic loudspeaker. *Building Acoustics*, 30(3):249–263, 2023.

[18] Maxime Morell, Manuel Collet, Emmanuel Gourdon, and Alireza Ture Savadkoohi. Control of an acoustic mode by a digitally created Nonlinear Electroacoustic Absorber at low excitation levels: Analytical and Experimental results. In *Surveillance, Vibrations, Shock and Noise*, 2023.

[19] Maxime Morell, Emanuele De Bono, Manuel Collet, Emmanuel Gourdon, and Alireza Ture Savadkoohi. An Electroacoustic Absorber featuring Nonlinear dynamics at low excitation amplitudes. In *SPIE Smart Structures + NDE*, 2021.

[20] M. Morell, E. Gourdon, M. Collet, A. Ture Savadkoohi, and E. De Bono. Nonlinear Digitally created Electroacoustic Absorber Designed for Acoustic Energy Pumping. pages 4807–4810, 2024.

[21] Sami Karkar, Emanuele De Bono, Manuel Collet, Gaël Matten, Morvan Ouisse, and Etienne Rivet. Broadband Nonreciprocal Acoustic Propagation Using Programmable Boundary Conditions: From Analytical Modeling to Experimental Implementation. *Physical Review Applied*, 12(5):054033, nov 2019.

[22] Emanuele De Bono, Manuel Collet, and Morvan Ouisse. The Advection Boundary Law in absence of mean flow: passivity, nonreciprocity and enhanced noise transmission attenuation. *arXiv preprint arXiv:2403.10426*, 2024.

[23] Emanuele De Bono, Morvan Ouisse, Manuel Collet, Edouard Salze, and Jacky Mardjono. A nonlocal boundary control, from plane waves to spinning modes control. In *Active and Passive Smart Structures and Integrated Systems XVII*, volume 12483, page 74. SPIE, 2023.

[24] É. Salze, E. De Bono, K. Billon, M. Gillet, M. Volery, M. Collet, M. Ouisse, H. Lissek, and J. Mardjono. Electro-active acoustic liner for the reduction of turbofan noise. In *Forum Acusticum*, pages 6057–6060, 2024.

[25] K. Billon, E. De Bono, M. Perez, E. Salze, G. Matten, M. Gillet, M. Ouisse, M. Volery, H. Lissek, J. Mardjono, and M. Collet. In flow acoustic characterisation of a 2D active liner with local and non local strategies. *Applied Acoustics*, 191:108655, 2022.

[26] Kevin Billon, Emanuele De Bono, Matthias Perez, Edouard Salze, Gaël Matten, Martin Gillet, Morvan Ouisse, Maxime Volery, Hervé Lissek, Jacky Mardjono, and Manuel Collet. Experimental assessment of an active (acoustic) liner prototype in an acoustic flow duct facility. In *Health Monitoring of Structural and Biological Systems XV*, volume 11593, page 84. International Society for Optics and Photonics, 2021.

[27] Kevin Billon, Manuel Collet, Edouard Salze, Martin Gillet, Morvan Ouisse, Maxime Volery, Hervé Lissek, and Jacky Mardjono. 2D active liner experimental results in acoustic flow duct facility. In *Smart Materials, Adaptive Structures and Intelligent Systems*, volume 86274, page V001T03A001. American Society of Mechanical Engineers, 2022.

[28] Kevin Billon, Martin Gillet, Edouard Salze, Maxime Volery, Emanuele De Bono, Morvan Ouisse, Herve Lissek, Manuel Collet, and Jacky Mardjono. Smart acoustic lining for UHBR technologies engine: from the design of an electroacoustic metasurface to experimental characterization under flow. In *Active and Passive Smart Structures and Integrated Systems XVII*, volume 12483, page 72. SPIE, 2023.

[29] Philip McCord Morse and K Uno Ingard. *Theoretical acoustics*. Princeton university press, 1986.

[30] Jacob Pieter Den Hartog. *Mechanical vibrations*. Courier Corporation, 1985.

[31] G B Warburton and E O Ayorinde. Optimum absorber parameters for simple systems. *Earthquake Engineering & Structural Dynamics*, 8(3):197–217, 1980.

[32] K L Hong and J Kim. New analysis method for general acoustic-structural coupled systems. *Journal of sound and vibration*, 192(2):465–480, 1996.

[33] Mehmet Bulent Ozer and Thomas J Royston. Application of Sherman–Morrison matrix inversion formula to damped vibration absorbers attached to multi-degree of freedom systems. *Journal of sound and vibration*, 283(3-5):1235–1249, 2005.

[34] Mehmet Bulent Ozer and Thomas J Royston. Extending Den Hartog's vibration absorber technique to multi-degree-of-freedom systems. 2005.

[35] Mariana M Americano da Costa, Daniel A Castello, Carlos Magluta, and Ney Roitman. On the optimal design and robustness of spatially distributed tuned mass dampers. *Mechanical Systems and Signal Processing*, 150:107289, 2021.

[36] Elyes Mrabet, Mohamed Najib Ichchou, and Noureddine Bouhaddi. Random vibro-acoustic control of internal noise through optimized Tuned Mass Dampers. *Mechanical Systems and Signal Processing*, 130:17–40, 2019.

[37] Etienne Rivet, Sami Karkar, and Hervé Lissek. On the optimisation of multi-degree-of-freedom acoustic impedances of low-frequency electroacoustic absorbers for room modal equalisation. *Acta Acustica United With Acustica*, 103(6):1025–1036, 2017.

[38] Vu Thach Pham. Sound Field Reconstruction in a room through Sparse Recovery and its application in Room Modal Equalization. Technical report, EPFL, 2021.

[39] A. Moiola, R. Hiptmair, and I. Perugia. Plane wave approximation of homogeneous Helmholtz solutions. *Zeitschrift fur Angewandte Mathematik und Physik*, 62(5):809–837, 2011.

[40] E Rice. Modal propagation angles in ducts with soft walls and their connection with suppressor performance. In *5th Aeroacoustics Conference*, page 624, 1979.

[41] Philip M Morse. Some aspects of the theory of room acoustics. *The Journal of the Acoustical Society of America*, 11(1):56–66, 1939.

[42] Sjoerd W Rienstra. Fundamentals of duct acoustics. *Von Karman Institute Lecture Notes*, 2015.